City, University of London Institutional Repository

Durham Research Online

A unique Critical State two-surface hyperplasticity model for fine-grained particulate media

W.M. Coombs[a,*], R.S. Crouch[a], C.E. Augarde[a]

[a]*Durham University, School of Engineering & Computing Sciences, Science Site, South Road, Durham, DH1 3LE, UK.*

Abstract

Even mild compression can cause re-arrangement of the internal structure of clay-like geomaterials, whereby clusters of particles rotate and collapse as face-to-face contacts between the constituent mineral platelets increase at the expense of edge-to-face (or edge-to-edge) contacts. The collective action of local particle re-orientation ultimately leads to path-independent isochoric macroscopic deformation under continuous shearing. This asymptotic condition is *the* governing feature of Critical State elasto-plasticity models. Unlike earlier formulations, the two-surface *anisotropic* model proposed herein is able to reproduce a unique isotropic Critical State stress envelope which agrees well with test data. Material point predictions are compared against triaxial experimental results and five other existing constitutive models. The hyperplastic formulation is seen to offer a significantly improved descriptor of the anisotropic behaviour of fine-grained particulate materials.

Keywords:

Two-surface anisotropy, hyperplasticity, Critical State, implicit stress integration, algorithmic tangent

1. Critical State geomechanics

In the context of continuum idealisations of the deformation of particulate media, the term constitutive model is a misnomer. For example, current models for soils generally demand little or no information about the mineralogy, grain geometry or packing. Instead they request parameters largely obtained from axi-symmetric tests which make no direct investigation of the fabric. Despite this, if constructed in a thermodynamically consistent manner with experimentally de-

termined values for the material constants, spatially averaged continuum representations can satisfactorily simulate the distortion, dilation and compaction of aggregated clusters of mineral platelets.

One of the more successful and widely used constitutive formulations for fine-grained geomaterials (in particular, clay-like soils) is the isotropic modified Cam-clay (MCC) plasticity model, proposed by Roscoe and Burland (1968). Central to this model (and subsequent extensions) is the concept of a Critical State (CS), initially proposed by Casagrande (1936), where the medium undergoes unbounded distortions at constant stress and volume. However, isotropic models are unable to account for the preferred orientation of the fabric which can have a pronounced influence on stiffness and strength. Thus a number of extensions to the MCC plasticity model have been proposed to represent this directional bias. These introduce some form of plastic anisotropy through rotation and/or shearing of the yield surface (for example see Belokas and Kavvadas (2010); Dafalias (1986); Gajo and Wood (2001); Karstunen and Koskinen (2008); Karstunen et al. (2005); Pestana and Whittle (1999); Sivasithamparam et al. (2010); Wheeler et al. (2003); Whittle and Kavvadas (1994)).

Earlier anisotropic extensions to the MCC model failed to include both (i) a unique convex CS surface dependent on both the intermediate principal stress and Lode angle and (ii) hysteretic behaviour during unloading and reloading. Those shortcomings are addressed in the hyperplastic formulation described here. The new model exhibits an asymptotic isochoric state which is uninfluenced by any initial or evolving anisotropy, and is independent of the path followed. This is consistent with findings from classical experimental work undertaken by Casagrande (1936); corroborated repeatedly thereafter by many workers on many different soils. Casagrande's CS represents a statistically averaged condition associated with large shear distortions, whereby particle clusters reorganize themselves to globally balance volume-reduction with volume-dilation, while the degree of anisotropy and the components of the stress tensor reach a stationary state.

The layout of the paper is as follows. Sections 2 and 3 describe the structure of clay and key findings from discrete element analyses respectively. These observations are used in Section 4 to develop the new two-surface anisotropic elasto-plasticity model. The complete model formulation is described, the key constitutive equations provided and a method for calibrating the model given. Section 5 is concerned with the algorithmic treatment of the model. In Section 6, the performance of the new model is assessed against five existing models based on Critical State soil mechanics (including the classical MCC model) and compared with experimental data on Lower Cromer Till (LCT) from Gens (1982). Predictions from the proposed and MCC models are also

2

compared under a rotating deviatoric strain field in Section 7. Final conclusions are drawn in Section 8.

2. The structure of clay

Fine grained clay minerals typically comprise hydrous aluminium phyllosilicates (weathered feldspars) falling within one of four major groups: kaolin, smectite, illite and chlorite (Brindley and Brown (1980)). The particles have a sheet-like morphology (Bennett et al. (1990)). Multiple platelets form domains through being attached in edge-to-edge, edge-to-face or stacked face-to-face configurations. Domains may group together to form flocculated clusters as a consequence of van der Waals attraction and edge-to-face double-layer repulsion. On a larger scale, clusters can group together to form peds (Holfz and Kovacs (1985)). On the (granular) scale of clusters and peds, frictional forces control the mechanics rather than electrostatic or van der Waals forces.

3. Discrete element findings

Since the pioneering work of Cundall and Strack (1979), discrete element models (DEM) have provided valuable insights when analyzing the mechanical behaviour of granular media. However, prior to the first DEM studies, Horne (1965a,b) investigated the theoretical behaviour of rotund, rigid, cohesionless particles[1]. The work offered the following conclusion regarding the response of granular material within a triaxial cell:

> *"... the complete behaviour in the triaxial test may be explained in terms of an induced degree of anisotropy which increases to a maximum close to the peak stress ratio, subsequently decreasing until the condition of no further volume change causes the degree of anisotropy to become stabilized."*

That is, the material anisotropy reaches an asymptotic value, as the stress state approaches a limiting stress ratio, q/p, at the CS[2]. Horne's analytical work was based on spherical particles. An extension of the theory to consider elongated platelets found in clay has not yet been made.

---

[1]Horne's work ignored the effect of elastic/plastic deformation, crushing and cracking, assuming that the deformation occurs as a result of the relative motion between groups of particles.

[2]Where $p = \sigma_{ii}/3$ is the hydrostatic pressure and $q = \sqrt{s_{ij}s_{ij}}$ is a scalar measure of the deviatoric stress with $s_{ij} = \sigma_{ij} - p\delta_{ij}$ and δ_{ij} is the *Kronecker delta* tensor.

Recent DEM-based studies have attempted to explore the uniqueness of the CS. Rothenburg and Kruyt (2004) analysed 5×10^4 circular discs. The results indicated that the CS is linked to a threshold number of contacts per particle, itself governed by interparticle friction. Nouguier-Lehon et al. (2003) used a range of particle shapes to study the CS; noting that the way that anisotropy changes during shearing is strongly influenced by particle shape and angularity. It was concluded that limiting anisotropy was reached when attaining a CS. Peña et al. (2009, 2007) also presented a study which focussed on the uniqueness of the CS. In these simulations, the stress ratio and void ratio evolved towards the same critical values, independently of the initial anisotropy. Studies by Fu and Dafalias (2011a,b) again confirmed the uniqueness of the CS for anisotropic granular materials, although the material was shown to be at the CS only in localized zones (shear bands). In their 2011 paper, those authors concluded that:

> "...a common ultimate state in terms of fabric characteristics is reached at large strains regardless of the initial fabrics prior to shear deformation. ...A direct implication of this conclusion is the uniqueness of the critical state line in the e-p [void ratio-pressure] space..."

They also found that the inclination of the anisotropy at the CS did not coincide with the shear band but instead was at some inclination "...between the shear band direction and the minor principal stress direction" (Fu & Dafalias 2011).

While continuum idealisations of the bulk material still provide the most appropriate approach for engineers designing large-scale structures, the findings from DEM, such as (i) the uniqueness of the CS and (ii) residual anisotropy at that state, provide valuable guidance when developing continuum constitutive models.

4. Anisotropic constitutive formulation

The fundamental assumption used in hyperplastic continuum formulations is that the constitutive equations can be derived from a free-energy function and a rate of dissipation function. Once these have been specified, the stress-elastic strain law, yield function and flow rule can all be obtained without the requirement for any additional assumptions. Textbook accounts of the thermomechanics of materials can be found in the volumes by Ziegler (1983) and Maugin (1992), amongst others.

4.1. Hyperelastic free-energy function

Particulate geomaterials typically demonstrate a dependence of the elastic bulk modulus on the current effective pressure, or equivalently on the current elastic volumetric strain. One common approach is to specify the elastic shear modulus directly from the bulk modulus assuming a constant Poisson's ratio, Gens and Potts (1988). However, this leads to a non-linear elasticity model in which energy can be generated from certain loading cycles (Borja and Tamagnini (1998); Houlsby (1985); Zytynski et al. (1978)). In this paper use is made of a variable bulk modulus with a constant shear modulus, as proposed by Houlsby (1985). This can be realised by adopting an elastic free-energy function of the form

$$\Psi_1 = \kappa p_r \exp\left(\frac{\varepsilon_v^{\mathrm{e}} - \varepsilon_{v0}^{\mathrm{e}}}{\kappa}\right) + G\left(\gamma_{ij}^{\mathrm{e}} \gamma_{ij}^{\mathrm{e}}\right) \tag{1}$$

with $\varepsilon_v^{\mathrm{e}} = \varepsilon_{ii}^{\mathrm{e}}$ and $\gamma_{ij}^{\mathrm{e}} = \varepsilon_{ij}^{\mathrm{e}} - \varepsilon_v^{\mathrm{e}}\delta_{ij}/3$, where $\varepsilon_{ij}^{\mathrm{e}}$ is the elastic strain tensor, κ is the bi-logarithmic elastic compressibility index, G is the constant shear modulus, p_r is the reference pressure and $\varepsilon_{v0}^{\mathrm{e}}$ is the elastic volumetric strain at that reference pressure. Note that repeated subscripts imply summation in the normal fashion. The true, Cauchy, stress (σ_{ij}) is given by the first derivative of (1) with respect to the elastic strain tensor. The non-linear elastic stiffness tensor is obtained from the second derivative of (1) with respect to elastic strain.

4.2. Rate of dissipation

The following dissipation rate is used to define the inelastic constitutive behaviour

$$\dot{\Phi} = \underbrace{\sqrt{(\dot{\varepsilon}_{v_1}^{\mathrm{p}} + \beta_{ij}\dot{\gamma}_{ij_1}^{\mathrm{p}})^2 A^2 + (\dot{\varepsilon}_{\gamma_1}^{\mathrm{p}} B)^2}}_{\dot{\Phi}_1} + \underbrace{\sqrt{(\dot{\varepsilon}_{v_2}^{\mathrm{p}} + \beta_{ij}\dot{\gamma}_{ij_2}^{\mathrm{p}})^2 A_f^2 + (\dot{\varepsilon}_{\gamma_2}^{\mathrm{p}} B_f)^2}}_{\dot{\Phi}_2}, \tag{2}$$

where $\dot{\Phi}_1$ and $\dot{\Phi}_2$ are the additive rates of dissipation associated with the inelastic material behaviour, $\dot{\varepsilon}_v^{\mathrm{p}} = \dot{\varepsilon}_{ii}^{\mathrm{p}}$, $\dot{\gamma}_{ij}^{\mathrm{p}} = \dot{\varepsilon}_{ij}^{\mathrm{p}} - \dot{\varepsilon}_v^{\mathrm{p}}\delta_{ij}/3$, $\dot{\varepsilon}_\gamma^{\mathrm{p}} = \sqrt{\dot{\gamma}_{ij}^{\mathrm{p}}\dot{\gamma}_{ij}^{\mathrm{p}}}$ and $\dot{\varepsilon}_{ij}^{\mathrm{p}}$ is the tensorial rate of plastic straining. β_{ij} controls the dissipative cross-coupling of the volumetric and deviatoric plastic strain rates. A, B, A_f and B_f are stress-like quantities that contain information on the previous history and the current stress state of the material.

The first component of the dissipation rate, $\dot{\Phi}_1$, was initially introduced by Collins and Hilder (2002) as an extension to their isotropic family of CS models. However, the model was only presented conceptually, and was limited to the axi-symmetric triaxial case. $\dot{\Phi}_1$ is similar to that proposed by Muhunthan et al. (1996) who introduced a cross-coupling in the dissipation

expression for the MCC model. Such single-surface models fail to capture the progressive plastic strains which can occur within the conventional yield surface[3]. $\dot{\Phi}_2$ in (2) is introduced to account for this dissipation. Following the procedure outlined by Collins (2003), and later used by Coombs and Crouch (2011), the inner surface is obtained as

$$f = (p - p^\chi)^2 B_f^2 + \left(s_{ij}^\beta s_{ij}^\beta\right) A_f^2 - A_f^2 B_f^2 = 0, \tag{3}$$

where $s_{ij}^\beta = (s_{ij} - s_{ij}^\chi - (p - p^\chi)\beta_{ij})$ is a local measure of the deviatoric stress from the axis of the inner yield surface (see Figure 1). $p^\chi = \sigma_{ii}^\chi/3$ and $s_{ij}^\chi = \sigma_{ij}^\chi - p^\chi \delta_{ij}$ are the hydrostatic and deviatoric *shift* stresses which locate the *centre* of the inner yield surface, σ_{ij}^χ. The coupling of volumetric and deviatoric plastic strains in the dissipation function (2), controlled by β_{ij}, results in a deviatoric (anisotropic) shearing of the yield surface. The cross-coupling reflects the fact that the shearing of soil leads to dilation or compaction as a result of clusters of particles sliding over one another. The yield surface resulting from $\dot{\Phi}_1$ is used to control the movement on the inner surface and provides a measure of the material's past history, whereas f from $\dot{\Phi}_2$ captures the recent stress history of the material.

The parameters A_f and B_f are given by

$$A_f = (1-\gamma)(p-p^\chi) + (2-\gamma)\gamma R p_c/2 \quad \text{and} \quad B_f = \bar{\rho}(\theta)M\left((1-\alpha)(p-p^\chi) + \gamma R p_c/2\right), \tag{4}$$

where p_c is the hydrostatic size of the outer surface, M is the classical gradient of the Critical State line (CSL) in p-q stress space, $\bar{\rho}(\theta)$ controls the Lode angle dependency (LAD) of the surface and the constant $R \in [0, 1]$ is the ratio of the size of the inner and outer yield surfaces[4]. α and γ determine the shape of the surface (as shown by Coombs and Crouch (2011) for the case when $\beta_{ij} = 0$). If $R = 1$ then $p^\chi = \gamma p_c/2$ and $s_{ij}^\chi = \gamma p_c \beta_{ij}/2$; that is, the inner and outer surfaces coincide. The form of A_f and B_f ensure that the yield function, (3), has real roots regardless of the level of anisotropy. Solving (3) in terms of the deviatoric stress, we find that $A_f^2 - (p - p^\chi)^2 \geq 0$ must be satisfied. For given values of p^χ and p_c (and fixed material constants R and γ), the minima of $A_f^2 - (p - p^\chi)^2$ are located at the least compressive ($p = p^\chi - \gamma R p_c/2$) and most compressive ($p = p^\chi + (1 - \gamma/2)R p_c$) limits of the inner yield envelope. At these states

---

[3]The yield surface, f, provides a geometric representation of the rate of dissipation function; describing a boundary between elastic ($f < 0$) and elasto-plastic material behaviour ($f = 0$).

[4]The stress-like quantities associated with the outer surface dissipation, $\dot{\Phi}_1$, are given by $A = (1-\gamma)p + \gamma p_c/2$ and $B = M\left((1-\alpha)p + \alpha\gamma p_c/2\right)$ Collins and Hilder (2002).

we find $A_f = (p - p^\chi)$.

Ignoring the dependence of constitutive relations on the third invariant of stress can lead to significant over-estimation of the stiffness in geotechnical analyses (Coombs et al. (2010); de Souza Neto et al. (2008); Potts and Zdravković (2001)). A number of LADs have been proposed in the literature (for example see Bardet (1990); Bhowmik and Long (1990); Coombs et al. (2010); Lade and Duncan (1973); Matsuoka and Nakai (1974); Shield (1955); Willam and Warnke (1974)). Collins (2003) combined the Matsuoka-Nakai (M-N) yield condition with the CS cone by re-defining q in the *spatially mobilised plane* (see Matsuoka and Nakai (1974)). However, implementing the M-N deviatoric yield criterion in this manner constrains the admissible principal stress states to be compressive. This can cause difficulties when using an elastic predictor-plastic corrector stress integration scheme. Here we follow an alternative approach by introducing the Willam-Warnke (W-W) LAD (Willam and Warnke (1974)) into the constitutive equations through B_f from (3). To ensure convexity, the Lode angle is a local quantity based on the deviatoric stress measured (s_{ij}^β) from the anisotropic axes of the surfaces, as shown in Figure 1 (ii). The Lode angle for the inner surface is calculated from (A.1).

As discussed by Collins and Houlsby (1997), the plastic strain increment is given by a normal flow rule in *dissipative stress space*. This only implies an associated model in *true stress space* under the condition that the dissipation rate is independent of the true stress, σ_{ij}[5]. The product of the dissipative stress with the plastic strain rate gives the rate of energy dissipation, $\dot{\Phi}$. The direction of plastic flow in dissipative stress space is obtained by taking the derivative of the instantaneous dissipative yield surface with respect to dissipative stress. The resulting rate of plastic straining and the direction of plastic flow in true stress space are

$$\dot{\varepsilon}_{ij}^{\mathrm{p}} = \dot{\gamma} \underbrace{\left(\frac{2}{3} \Big(B_f^2 (p - p^\chi) - A_f^2 s_{kl}^\beta \beta_{kl} \Big) \delta_{ij} + 2 A_f^2 s_{ij}^\beta \right)}_{\text{direction of plastic flow, } (g_{,\sigma})_{ij}}, \tag{5}$$

where $\dot{\gamma} \geq 0$ is the plastic consistency parameter[6] satisfying the Kuhn-Tucker-Karush (KTK) conditions: $\dot{\gamma} \geq 0$, $f \leq 0$ and $\dot{\gamma} f = 0$.

---

[5]For the rate of dissipation function (2) an associated flow rule is obtained when $\alpha = \gamma = 1$ and $\bar{\rho}(\theta) = 1$. That is, when the terms dependent on the true stress, σ_{ij}, disappear from the stress-like quantities A, B, A_f and B_f.

[6]Not the rate of the γ parameter first seen in (4).

4.3. Isotropic hardening/softening

The hydrostatic measure p_c controls both the size of the outer and inner (through R) surfaces. Here, following Coombs and Crouch (2011), the rate of the evolution of the size of the outer surface is defined as

$$\dot{p}_c = \left(\frac{p_c}{\lambda - \kappa}\right)\dot{\varepsilon}_v^{\mathrm{p}}, \tag{6}$$

where λ is the plastic compressibility index[7]. This hardening law is equivalent to specifying a bi-logarithmic linear relationship between specific volume and pre-consolidation pressure (Borja and Tamagnini, 1998). The limitations of the conventional linear relationship between specific volume (or void ratio) and the logarithm of the pre-consolidation pressure were identified by Butterfield (1979). More recently, the appropriateness of the bi-logarithmic law for finite deformation analysis was verified by Hashiguchi (2008) and used by Yamakawa et al. (2010).

4.4. Anisotropic hardening and the Critical State

The anisotropic two-surface model allows the yield surface axes to orientate away from the direction of the hydrostatic axis, via a non-zero β_{ij} (see Figure 1). In the description of the model thus far, no discussion has been made on how the degree and direction of anisotropy changes with respect to inelastic straining. With the yield surface and direction of plastic flow suggested above, unless the level of anisotropy (β_{ij}) reduces to zero when approaching the CS, the original isotropic CS surface will be lost and the stress ratio at that *final* CS becomes dependent on the stress path taken to reach that state. To correct this, use is made of the following anisotropic hardening relationship, initially proposed by Wheeler et al. (2003)

$$\dot{\beta}_{ij} = C_\beta\Big(\big(r_{ij} - \beta_{ij}\big)\langle\dot{\varepsilon}_v^{\mathrm{p}}\rangle + x_\beta\big(b_\beta r_{ij} - \beta_{ij}\big)\dot{\varepsilon}_\gamma^{\mathrm{p}}\Big), \tag{7}$$

where $\langle(\cdot)\rangle$ is the ramp function of $(\cdot)$[8]. The local stress ratio, r_{ij}, is defined as the deviatoric to volumetric stress ratio measured from the apex of the inner yield surface (see Figure 1), given

---

[7]The plastic compressibility index, λ, is the bi-logarithmic slope of the specific volume versus hydrostatic pressure response under virgin hydrostatic drained compression.

[8]Note, that the original form of the hardening law proposed by Wheeler et al. (2003) contained a scalar multiplication term, a_β, on the first r_{ij}. That form of hardening law has since been used in several models, namely the S-CLAY1 and S-CLAY1S (Karstunen and Koskinen (2008); Karstunen et al. (2005)), BSCLAY (Sivasithamparam et al. (2010)), amongst others. Here, use is made on the simplified version of Wheeler et al. (2003) hardening law proposed by Coombs (2011), where the mutliplication on the first r_{ij} in (7) is unity.

8

by

$$r_{ij} = \frac{s_{ij}^r}{p_\beta} = \frac{s_{ij} - s_{ij}^\chi + (Rp_c\gamma/2)\beta_{ij}}{p - p^\chi + Rp_c\gamma/2} \tag{8}$$

The plastic volumetric strains in (7) drag the current level of anisotropy towards the target value of r_{ij}. The motivation for this change in β_{ij} follows the same argument given by Wheeler et al. (2003):

> "...plastic volumetric strains, involving slippage at inter-particle or inter-ped contacts, result in a gradual rearrangement of the soil fabric towards a configuration that has a degree of anisotropy that is controlled by the anisotropy of the stress state under which this plastic straining is occurring."

The use of a ramp function in (7) removes the influence of dilative plastic volumetric straining on the anisotropy of the material fabric. Note that unlike the previous work on anisotropic hyperplasticity conducted by Collins and co-workers (for example Collins and Hilder (2002)), here an injective function is not specified between the inelastic strains and anisotropy. In general, it is more appropriate for both the direction and level of anisotropy at a particular state to depend on the stress (and strain) path taken to reach that state.

Deviatoric plastic strains[9], $\dot{\varepsilon}_\gamma^p$, drag the current level of anisotropy towards a different target value of anisotropy given by $b_\beta r_{ij}$.

In (7), the material constant x_β specifies the relative contribution from the volumetric and deviatoric plastic strains and C_β scales the absolute rate of evolution. When approaching the CS, the volumetric component of plastic flow reduces and the development of β_{ij} is controlled by the deviatoric plastic strains. In the limiting case, where $\dot{\varepsilon}_v^p = 0$ under continued inelastic shearing, the rate of anisotropic evolution disappears $\dot{\beta}_{ij} \to 0$. Combining these conditions with (7), the unique level of anisotropy at the CS (referred to here as the Critical Anisotropy State, CAS) becomes $b_\beta(r_{cs})_{ij}$, where $(r_{cs})_{ij}$ is the local stress ratio at the CS. When $b_\beta \neq 0$, the value of M required to maintain the original p-q stress ratio at the CS, η_{cs}, is obtained from η_{cs}, γ, α and b_β (B.2). In the two-surface model (unlike the MCC model), M is a constant used to obtain the appropriate CS stress ratio, η_{cs}, rather than the gradient of the CSL itself. The anisotropy of the yield surface at the CS is thus independent of both (i) the initial anisotropy and (ii) the

---

[9]Note, that unlike the Wheeler et al. (2003) hardening law, constructed in triaxial p-q stress space, the modulus sign is not required on the deviatoric plastic strain rate as $\dot{\varepsilon}_\gamma^p$ is the L2 norm of the deviatoric plastic strain rate $\dot{\gamma}_{ij}^p$.

stress path taken to the reach this state. The residual *fabric* anisotropy at the CS also results in a unique CSL in the void ratio versus $\log(p)$ plane. The majority of previous formulations that include anisotropic shearing of the yield surface do not predict a unique CAS[10]. One exception is the S-CLAY1 model of Wheeler et al. (2003) (and subsequent extensions), although that model was confined to an elliptic yield surface based on the work of Dafalias (1986). Such a surface places restrictions on the level of anisotropy allowed to develop[11]. It also poses problems when implementing a generalised LAD. For example, while the shapes of the deviatoric cross sections of the yield surface are geometrically similar at different levels of hydrostatic stress, concavity of the surface can occur when $\beta_{ij} \neq 0$ (for example see Crouch and Wolf (1995)). This limitation has resulted in users of Dafalias' (1986) yield surface introducing a LAD on the plastic potential surface rather than the yield surface (for example see Dafalias et al. (2006)).

From the yield function and the direction of plastic flow, the position of the CS (in terms of the mean stress, p) relative to the size of the yield surface is given by (B.1) where $(p_a)_{cs} = p_s/p$. The position of the CS on the outer surface is a simple function of p_c, b_β and γ.

4.5. Movement of the inner surface

The concept of a projection (or similarity) centre, σ_{ij}^0, is adopted in the new model to control the motion, growth in size and change in shape of the inner surface. The use of a similarity centre was formalised by Hashiguchi (1988) for the subloading surface plasticity model to ensure that the inner surface remains geometrically similar to its outer surface. This projection centre is defined as the intersection point between rays linking common normals on the inner and outer surfaces. Such a construction maintains a constant ratio between the distances from the similarity centre to the yield surface and the yield to the outer surface along any ray emanating from the projection centre (see Figure 1).

From geometric considerations, the *centre* of the inner yield surface is linked to the projection centre through

$$\sigma_{ij}^\chi = (1 - R)\sigma_{ij}^0 + \frac{Rp_c\gamma}{2}\big(\delta_{ij} + \beta_{ij}\big), \tag{9}$$

where $p_c\gamma\delta_{ij}/2$ locates the centre of the outer surface. The following evolution rule for the

---

[10]This is the case for the anisotropic hardening laws which depend purely on plastic volumetric strains, such as those used by Dafalias (1986) and Whittle and Kavvadas (1994).

[11]The level of anisotropy for Dafalias (1986)'s yield surface is limited to $\beta < M$. When $\beta = M$ the surface deviatoric radius drops to zero and the yield surface becomes a line coincident with the CSL.

projection centre is used

$$\dot{\sigma}_{ij}^0 = C_\chi ||\dot{\varepsilon}_{ij}^{\mathrm{P}}||(\sigma_{ij} - \sigma_{ij}^0) + \frac{\dot{\varepsilon}_v^{\mathrm{P}}}{(\lambda - \kappa)}\sigma_{ij}^0 + p^0\dot{\beta}_{ij}, \tag{10}$$

where p^0 gives the hydrostatic pressure of the projection centre. The first term translates the inner surface towards the image point, $\breve{\sigma}_{ij}$, on the outer surface at a rate controlled by C_χ. This translation rule means that the inner surface can touch the outer surface but never overlap it. The rate of anisotropic shearing is scaled by the projection centre hydrostatic pressure to ensure that under plastic straining the centre of similarity translates appropriately, remaining consistent with the evolving anisotropy of the geometrically similar surfaces. The second term causes the projection centre to scale uniformly, from the origin, with isotropic expansion or contraction of the yield and outer envelopes. The first two terms in (10) are equivalent to those used by Mróz and Norris (1979), although here, as with the work of Rouainia and Wood (2001) and Belokas and Kavvadas (2010), we assume a constant ratio, R, between the sizes of the inner and outer surfaces.

Taking the rate of (9), substituting (10) and rearranging and simplifying, the resulting expression gives the following rate relationship for the evolution of the centre of the inner surface

$$\dot{\sigma}_{ij}^\chi = C_\chi ||\dot{\varepsilon}_{ij}^{\mathrm{P}}||\Big((1-R)\sigma_{ij} + Rp_c\gamma(\delta_{ij} + \beta_{ij})/2\Big) + \sigma_{ij}^\chi\Big(\dot{\varepsilon}_v^{\mathrm{P}}/(\lambda - \kappa) - C_\chi ||\dot{\varepsilon}_{ij}^{\mathrm{P}}||\Big) + p^\chi\dot{\beta}_{ij}. \tag{11}$$

4.6. Complete model formulation

Combining the elasticity law (from the free energy function (1)), yield function and direction of plastic flow (from the dissipation function (2)) and the hardening laws for the surface growth (6), shear anisotropy (7) and translation of the inner surface (11), gives all the constitutive relations needed for the two-surface anisotropic hyperplasticity model (a total of six equations). The infinitesimal elasto-plastic stiffness matrix is given in Appendix D along with the model's plastic consistency parameter and the plastic tangent stiffness.

4.7. Calibration

The complete set of material constants for the two-surface anisotropic model numbers 12. However, it is possible to reduce this to a smaller set of six primary parameters (κ, G, λ, M, C_β and C_χ), with the secondary six parameters ($\bar{\rho}_e$, R, α, γ, b_β and x_β) either assuming default values or being calculated directly from closed-form expressions. The classical MCC model requires four constants (κ, G, λ and M). Thus, only two additional primary constants

11

(controlling the rate of translation of the inner yield surface, C_χ, and the rate of development of anisotropy, C_β) require calibration for the two-surface model[12].

The set of six primary constants may be determined as follows: κ from the initial hydrostatic unloading or elastic loading, G from the initial one-dimensional straining (K_0) elastic unloading direction, λ using the virgin hydrostatic loading response, M from undrained triaxial compression to obtain η_{cs}, which is then used to calculate M through (B.2), C_χ using hydrostatic unloading or reloading (deviation from the bi-logarithmic κ line) and C_β from elasto-plastic K_0 unloading behaviour. Therefore, data from the following three experiments are all that are required to calibrate the material constants for the two-surface anisotropic model:

(i) hydrostatic loading, to provide λ, and unloading to give κ and C_χ;

(ii) a single undrained triaxial compression test to determine the stress ratio at the CS, η_{cs} (for M); and

(iii) K_0 loading, to supply η_{K_0} (for x_β), and unloading to provide G and C_β.

These three laboratory tests can be conducted relatively easily using a standard geotechnical apparatus.

Four of the secondary constants can assume the following default values: $\alpha = 0.6$, to reduce the over-prediction of the stress ratio at high over-consolidation ratios (OCRs)[13], $b_\beta = 0.1$, $\gamma = 0.89$, so that position of the CSL relative to the size of the yield surface is the same as for the MCC model (that is, $(p/p_c)_{cs} = 0.5$, see Coombs (2011) for details) and $R = 0.2$.

The two remaining secondary constants ($\bar{\rho}_e$ and x_β) require calculation by the user. The normalised deviatoric radius under triaxial extension can be obtained from η_{cs} using $\bar{\rho}_e = \sqrt{6}(\sqrt{6} + \eta_{cs})^{-1}$. The constant controlling the relative contributions of volumetric and deviatoric plastic straining on the development of anisotropy can be obtained from the stress ratio under one-dimensional drained K_0 loading, η_{K_0}, using

$$x_\beta = \frac{\eta_{K_0} - \beta_{K_0}}{n_p\big(\beta_{K_0} - b_\beta \eta_{K_0}\big)}, \tag{12}$$

---

[12] Previous extensions to the MCC model, such as the single-surface formulations of Karstunen et al. (2005) and Wheeler et al. (2003) require 8 constants whereas the more sophisticated two-surface models of Whittle and Kavvadas (1994) and Pestana and Whittle (1999) require 15 and 13 constants respectively. The recently proposed model of Sivasithamparam et al. (2010) requires 10 constants, however it has no LAD or control over the shape of the ellipsoidal yield surface, leading to strength over-predictions for both non-compressive load paths and over-consolidated soil states.

[13] The OCR is a measure of the previous stress history of the material, defined as the ratio between the previous maximum and current pressures.

where β_{K_0} is given in Appendix C and $n_p = \sqrt{2/3}$ is the ratio of the deviatoric to volumetric plastic strains under continued K_0 straining[14]. When further experimental data are available, five of the six secondary constants (α, b_β, γ, R and $\bar{\rho}_e$) could be tuned to improve the quality of the simulations (as described by Coombs (2011)). Note that all of the constants, with the exception of the shear modulus, G, are dimensionless.

5. Algorithmic treatment

The use of nonlinear constitutive models within a finite-element scheme (or other similar analysis programs) requires an incremental relationship between stress and strain. Here, the two-surface anisotropic model is integrated using the implicit backward Euler method. In the implemented algorithm, the elastic strains (ε_{ij}^e), incremental plasticity consistency parameter ($\Delta\gamma$), size of the outer surface (p_c), position of the inner yield surface (σ_{ij}^χ) and the anisotropy inherent in the surfaces (β_{ij}) are taken as the primary unknowns. Residuals are formed through the compatibility of the elastic, plastic and total strains, along with the hardening laws for p_c, σ_{ij}^χ and β_{ij} and the inner surface yield function (3). Details of the implemented algorithm, including the derivation of the algorithmic consistent tangent stiffness matrix, were provided by Coombs (2011).

6. Model comparisons with experiments

This section compares the performance of the two-surface anisotropic model with experimental data on LCT. LCT is a low-plasticity sandy silty-clay (specific gravity of 2.65). All of the experimental tests presented by Gens (1982) were on reconstituted samples. The mineralogy of these samples comprised principally quartz, with minor proportions of calcite and feldspar minerals. The clay fraction was mainly composed of calcite and illite with smaller components of smectite, kaolinite and chlorite. The material had a liquid limit, plastic limit and plasticity index of 25, 13 and 12 respectively[15]. Approximately 17% of the material was clay-sized (giving

---

[14]Note that in this paper ε_γ^p is defined as the L2 norm of the deviatoric plastic strain tensor resulting in $n_p = \sqrt{2/3}$ rather than 2/3 as often used in geotechnical literature.

[15]Note, that the plasticity index (the difference between the limit and plastic limits) is a measure of the amount of water that must be added to the soil to reduce its strength by a hundredfold. The plastic limit is defined as the moisture content at which the soil can be rolled out to a rod with diameter of 3mm without crumbling. The liquid limit is the moisture content at which a standard V-groove cut into the soil just closes when shaken using standard equipment.

an activity of 0.71[16]). The remainder was mainly composed of sand, with very little silt. Despite the low clay content, this constituent dominates the behaviour of the soil.

Comparisons are made between the two surface anisotropic hyperplastic model and five other models embracing Critical State soil mechanics, namely: (i) the classical MCC model (with the addition of a LAD), (ii) an anisotropic bounding surface model with no LAD (Borja et al., 2001), (iii) an anisotropic *bubble* model[17] (similar to those models introduced by Mróz and Norris (1979) and Rouainia and Wood (2000, 2001), albeit with a different energy-conserving elasticity law), (iv) SANIclay (Dafalias et al., 2006) and (v) the isotropic two-parameter hyperplastic model (Coombs and Crouch, 2011). For all of the simulations, the constitutive models started from a hydrostatic stress state with a reference pressure of 80kPa. The MCC model used the following material constants: $\kappa = 0.007$, $G = 18$MPa, $\lambda = 0.0447$, $M = 0.964$ and $\bar{\rho}_e = 0.729$. The two-surface anisotropic model's constants were set to: $\kappa = 0.005$, $G = 28$MPa, $\lambda = 0.0447$, $M = 0.921$ (from (B.2) with $\eta_{cs} = 0.964$), $C_\beta = 14$, $C_\chi = 3700$, $\bar{\rho}_e = 0.729$, $\alpha = 0.4$ and $\gamma = 0.78$ while the remaining constants assumed their default values ($\eta_{k_0} = 0.6$ giving $x_\beta = 4.8$ from (12)). Note that although κ, G and M are familiar to users of the MCC model, they require different interpretations in the two-surface model. The elastic constants will assume smaller (κ) and larger (G) values than typically adopted for the MCC model; this is a consequence of elastoplastic behaviour within the conventional (outer) yield surface. For the two-surface model, M is dependent on the degree of anisotropy at the Critical State in addition to α and γ. For LCT, this results in $M < \eta_{cs}$.

6.1. One-dimensional straining

The responses of the six models subject to one-dimensional compressive straining are shown in Figure 2 together with the experimental data from Gens (1982). The MCC, bounding surface and *bubble* models (Figures 2 (i), (iii) and (v)) show similar behaviour. Initially the hydrostatic stress state is located at A, on the compressive limit of the yield surfaces with $p_c = 80$kPa (as shown by the dashed lines). Under one-dimensional loading the stress state moves around the *nose* of the expanding yield surfaces and approaches a constant stress ratio, q/p, under continued straining, arriving at B'. For the three models the stress response under one-dimensional compressive

---

[16]The activity of a sample is defined as the plasticity index divided by the percentage of clay particles $\leq 2\mu m$ present.

[17]The *bubble* model examined here was obtained by simplifying the two-surface anisotropic model such that it had ellipsoidal inner and outer surfaces ($\alpha = \gamma = 1$) with the direction of their major axes coincident with the hydrostatic axis ($C_\beta = 0$).

straining is dominated by the gradient of the CS line, M. The stress response using these three models provides a poor approximation to the experimentally observed behaviour.

Upon unloading (as shown in Figure 3 (i)) the MCC model behaves elastically (from B' to C') until intersecting with the yield surface at C'. Thereafter the stress path moves around the softening yield surface to D'. Again the MCC model provides an unsatisfactory approximation to the experimental data, with a $> 400\%$ overestimate of the deviatoric stress between D and D' (that is, a difference of 62kPa).

The six constants required for the bounding surface model were calibrated such that on unloading to an OCR of 7, the numerically predicted deviatoric stress agreed with that observed experimentally (point D in Figure 3 (iii))[18]. However, the path followed to reach this state is unsatisfactory when compared to the experimental data. The stress path of the LAD *bubble* model (requiring seven material constants[19]) also fails to convincingly reproduce the observed material behaviour, mainly due to its unloading stress state (point B', Figure 3 (v)).

The stress paths for the SANIclay model (Figures 2-5 (ii)) were obtained from Dafalias et al. (2006). In that paper, the eight constants required for the model were obtained by calibration with LCT experimental data (Gens, 1982). However, the paper did not present the full one-dimensional loading and unloading stress path, allowing the model to start at a stress state in agreement with the experimental data for each of the individual undrained triaxial simulations without simulating the material's full stress history. Under one-dimensional loading Dafalias et al. (2006) only showed a straight η_{K_0} line alongside the material data (Figure 2 (ii)) and the initial unloading response (Figure 3 (ii)) between points B and C. It should be noted that the elasticity law for the SANIclay model used a pressure sensitive bulk modulus combined with a constant Poisson's ratio. As commented on in Section 4.1, this particular form of non-linear elasticity can give rise to a non-conservative response.

Using the same seven material parameters as those used by Coombs and Crouch (2011), the two-parameter α-γ model is able to capture the one-dimensional consolidation response of LCT, achieving the appropriate deviatoric stress at a hydrostatic pressure of 233kPa (point B in Figure 2 (iv)). However, the model is unable to convincingly reproduce the unloading behaviour, shown in Figure 3 (iv), significantly over estimating the change in deviatoric stress at D' when

---

[18]The material constants for Borja et al. (2001)'s bounding surface model were: $\kappa = 0.007$, $G = 6.2$MPa (no cross coupling between the bulk and shear moduli), $\lambda = 0.0447$, $M = 0.964$, $h = 5$MPa and $m = 1.5$.

[19]The *bubble* model's material constants were: $\kappa = 0.005$, $G = 28$MPa, $\lambda = 0.0447$, $M = 0.964$, $C_\chi = 3700$, $\bar{\rho}_e = 0.729$, $R = 0.2$

compared with the experimental over-consolidated state at D.

The response of the new two-surface model subjected to K_0 straining is shown in Figure 2 (vi). Initially there is zero anisotropy in the surface, with the stress state located at A on the *nose* of both the inner and outer surfaces, again with $p_c = 80\text{kPa}$ (as shown by the dashed lines in Figure 2 (vi)). Under the one-dimensional straining, the stress state initially moves round the *nose* of the hardening yield surface and approaches the K_0 stress ratio, η_{K_0}. Under continued K_0 loading, the surfaces moves away from the hydrostatic axis, introducing anisotropy into both the inner and outer surfaces, as shown for the stress state at B where the elastic region is shaded grey. At B the elastic and plastic strains in the direction of loading are 0.0039 and 0.0509 (that is, the plastic strain is 13 times larger than the elastic strain). The majority of the one-dimensional straining is associated with the re-arrangement and sliding of particles. Upon reversal of the K_0 straining direction, the stress state unloads elastically to C whereupon the model then undergoes further elasto-plastic deformation until reaching D, as shown in Figure 3 (vi). Excellent agreement is seen between the one-dimensional loading-unloading model response and the experimental data.

6.2. Undrained triaxial response

Figures 4 (i) and 5 (i) show the undrained triaxial compression (UTC) and extension (UTE) responses of the MCC model following one-dimensional loading and unloading, as described in the preceding sub-section. The constitutive model was subjected to strain increments $\Delta\varepsilon_{11} = \pm 1 \times 10^{-4}$, $\Delta\varepsilon_{22} = \pm 1 \times 10^{-4}$, $\Delta\varepsilon_{33} = \mp 2 \times 10^{-4}$ and $\Delta\varepsilon_{ij} = 0$ when $i \neq j$, until the CS was reached. Initially, under undrained compression, the stress state undergoes purely elastic deformation and moves in a deviatoric direction from D' to E'. Inelastic behaviour commences at E' and, under continued elasto-plastic deformation, the stress state moves around the yield surface, reaching the CS at F'. Although the final stress state of the MCC model (F') and the experimental observed behaviour of LCT (F) are similar, the K_0 starting states and stress paths taken are quite different. Under triaxial extension the MCC model undergoes elasto-plastic deformation from D' to G'. Again, the MCC model response provides a poor approximation to the observed experimental stress path (D to G).

The undrained stress paths of the bounding surface model also fail to reproduce the experimentally observed material behaviour. For any stress paths that involve *unloading*, the uniqueness of the CS is potentially lost as the inner loading surface jumps to the unloading stress state. It should also be noted, as observed by the authors of the model, that despite its robustness on

16

the compactive side of the CS line, the model is potentially numerically unstable under softening (Borja et al., 2001). In this study, it was not possible to advance the stress paths past points F' in Figure 4 (iii) and G' in Figure 5 (iii). However, if this numerical difficulty could be overcome, the model would predict a softening response (once the loading and bounding surfaces had converged) towards the CS, potentially achieving good agreement with the experimentally observed final stress state under UTC.

The stress paths in Figures 4 (ii) and 5 (ii) were obtained from Dafalias et al. (2006). The single-surface model's compressive stress path overestimates the deviatoric stress (point E') prior to reaching the CS, although it does capture the general material behaviour. The stress path under undrained triaxial extension diverges significantly from the experimentally observed behaviour and has a error of 52kPa in the final hydrostatic stress state at G' (an error of 55% between G and G').

Despite the unsatisfactory initial state when starting undrained triaxial compression or extension (D' in Figure 3 (iv)), the isotropic two-parameter model's (Coombs and Crouch, 2011) subsequent stress path qualitatively captures the observed material behaviour under both UTC, Figure 4 (iv), and UTE, Figure 5 (iv). In particular, due to the shape of the yield surface, the overestimation of the deviatoric stress seen in the MCC model is significantly reduced under both UTC and UTE. The stress paths of the LAD *bubble* model are shown in Figures 4 (v) and 5 (v). Both the undrained compression and extension stress paths over-estimate the deviatoric stress.

The response of the two-surface anisotropic model is shown in Figures 4 (vi) and 5 (vi). Starting at D, under triaxial compression the model initially undergoes purely elastic deformation. The two-surface model then exhibits elasto-plastic behaviour until the CS is attained at F. The yield surfaces distort such that at the CS stress ratio, η_{cs} (at F), the anisotropy, β, equals $b_\beta \eta_{cs}$. The stress path under UTE moves from D to G, where the stress ratio becomes equal to $\bar{\rho}_e \eta_{cs}$ and $\beta = b_\beta \bar{\rho}_e \eta_{cs}$. Good agreement is observed between the new two-surface model prediction and the experimentally observed material behaviour.

Figures 2-5 have demonstrated that the two-surface anisotropic model, unlike the other five models examined, is able to capture the undrained stress path history of the material satisfactorily using a single set of constants. The model's stress paths properly achieve a unique isotropic CS surface. The advantages of a two-surface formulation become even more noticeable when simulating multi-cyclic behaviour. The following section considers one such example.

7. Rotating strain path

The influence of anisotropy on a constitutive model's response when subjected to a strain path that changes the orientation of the principal stress directions is now illustrated. The MCC and two-surface anisotropic models were first uniaxially strained compressively (drained K_0 consolidation) to a hydrostatic pressure of 233.3kPa and then K_0 unloaded to a pressure of 200kPa. From this state both models were subjected to a rotating isochoric total strain path with a deviatoric radius of 1000 micro strains (that is, 1×10^{-3}) in half degree increments. This circular strain path was repeated 10 times. Figure 6 shows the one-dimensional loading (points A to B/B') and unloading (points B/B' to C/C') followed by the circular strain path response for the MCC model (dashed line) and the two surface anisotropic model (solid line). The responses are shown in (i) q versus p space and (ii) a three-dimensional normal stress space deviatoric view down the hydrostatic axis.

Under rotational straining the MCC model's behaviour is elastic, resulting in a circular stress path at a constant hydrostatic pressure of 200kPa. The two-surface anisotropic model's stress path reveals the influence of both the inclination of the yield surface and the presence of an inner surface. Under continued strain rotation, the effective hydrostatic pressure reduces and the inner surface translates towards the hydrostatic axis. The model asymptotically approaches a *stabilised* state with $p \to 116.2$kPa, $p^\chi \to 116.2$kPa, $\dot{\varepsilon}_v^{\mathrm{p}} \to 0$ and $\beta_{ij} \approx 0$ (the latter experiences small oscillations under the circular strain path). The important observation is that under this undrained rotational strain path, the MCC model fails to capture the build-up of excessive pore water pressure.

8. Conclusion

This paper has presented a complete anisotropic inelastic framework for the deformation of fine-grained particulate materials based on Critical State hyperplasticity and guided by discrete element findings (in particular, the uniqueness of the Critical State). The constitutive formulation implies that a fixed level of anisotropy is attained upon reaching the Critical State. The evolving anisotropy follows directly from a cross-coupling between the volumetric and deviatoric plastic strain rates in the rate of dissipation function. This anisotropy can be visualised as a shearing of the yield surfaces away from the hydrostatic axis. The use of a local Lode angle accounts for the dependence of the model on the intermediate principal stress. It also maintains the convexity of the yield envelopes. A further attractive feature of the formulation is that it is part of a family

of constitutive models that contains the modified Cam-clay model as a special case (see Coombs (2011)).

In the model's most general form, it requires the specification of 12 material parameters. However, six of these constants can take default values (R, α, γ and b_β) or be obtained from closed-form expressions ($\bar{\rho}_e$ and x_β) based on easily measured quantities using standard geotechnical laboratory equipment. The calibration procedure for the remaining six constants, including the classical κ, G, λ and M parameters plus C_β and C_χ, is described in Section 4.7. It has been shown that the proposed model is able to satisfactorily reproduce the multi-stage behaviour (for example K_0 consolidation and unloading followed by triaxial shearing) of a fine-grained soil using a single set of material constants. This two-surface anisotropic model improves upon the realism offered by existing anisotropic extensions to the MCC formulation.

References

Bardet, J., 1990. Lode dependences for isotropic pressure-sensitive elastoplastic materials. Transactions of the ASCE 57, 498–506.

Belokas, G., Kavvadas, M., 2010. An anisotropic model for structured soils part i: theory. Computers and Geotechnics 37, 737–747.

Bennett, R., Bryant, W., Hulbert, M., 1990. Microstructure of fine-grained sediments. Springer-Verlag.

Bhowmik, S., Long, J., 1990. A general formulation for the cross sections of yield surfaces in octahedral planes. In: Pande, G., Middleton, J. (Eds.), NUMENTA 90. pp. 795–803.

Borja, R., Lin, C., Montans, F., 2001. Cam-clay plasticity, part iv: Implicit integration of anisotropic bounding surface model with nonlinear hyperelasticity and ellipsoidal loading function. Comput. Methods Appl. Mech. Eng. 190, 3293–3323.

Borja, R., Tamagnini, C., 1998. Cam-clay plasticity part iii: Extension of the infinitesimal model to include finite strains. Comput. Methods Appl. Mech. Engrg. 155, 73–95.

Brindley, G., Brown, G. (Eds.), 1980. Crystal structures of clay minerals an their X-ray identification. Mineralogical Society, London.

Butterfield, R., 1979. A natural compression law for soils (an advance on e-logp'). Géotechnique 29 (4), 469–480.

Casagrande, A., 1936. Contributions to soil mechanics. Boston Society of Civil Engineers, Ch. Characteristics of cohesionless soils affecting the stability of slopes and earth fills, pp. 257–276.

Collins, I., 2003. A systematic proceedure for constructing critical state models in three dimensions. Int. J. Solids Struct. 40, 4379–7397.

Collins, I., Hilder, T., 2002. A theoretical framework for constructing elastic/plastic constitutive models of triaxial tests. Int. J. Numer. Anal. Meth. Geomech. 26, 1313–1347.

Collins, I., Houlsby, G., 1997. Application of thermomechanical principles to the modelling of geotechnical materials. Proc. R. Soc. Land. A 453, 1975–2001.

Coombs, W., 2011. Finite deformation of particulate geomaterials: frictional and anisotropic Critical State elasto-plasticity. Ph.D. thesis, Durham University.

Coombs, W., Crouch, R., 2011. Algorithmic issues for three-invariant hyperplastic critical state models. Comput. Methods Appl. Mech. Engrg. 200, 2297–2318.

Coombs, W., Crouch, R., Augarde, C., 2010. Reuleaux plasticity: analytical backward Euler stress integration and consistent tangent. Comput. Methods Appl. Mech. Engrg. 199, 1733–1743.

Crouch, R., Wolf, J., 1995. On a three-dimensional anisotropic plasticity model for soil. Géotechnique 45 (2), 301–305.

Cundall, P., Strack, O., 1979. A discrete numerical model for granular assemblies. Géotechnique 29, 47–65.

Dafalias, Y., 1986. An anisotropic critical state soil plasticity model. Mech. Res. Commun. 13, 341–347.

Dafalias, Y., Manzari, M., Papadimitriou, A., 2006. Saniclay: simple anisotropic clay plasticity model. Int. J. Numer. Anal. Meth. Geomech. 30, 1231–1257.

de Souza Neto, E., Perić, D., Owen, D., 2008. Computational methods for plasticity: Theory and applications. John Wiley & Sons Ltd.

Fu, P., Dafalias, Y., 2011a. Fabric evolution within shear bands of granular materials and its relation to critical state theory. Int. J. Numer. Anal. Meth. Geomech. 35, 1918–1948.

Fu, P., Dafalias, Y., 2011b. Study of anisotropic shear strength of granular materials using dem simulation. Int. J. Numer. Anal. Meth. Geomech. 35, 1098–1126.

Gajo, A., Wood, D., 2001. A new approach to anisotropic, bounding surface plasticity: general formulation and simulations of natural and reconstituted clay behaviour. Int. J. Numer. Anal. Meth. Geomech. 25, 207–214.

Gens, A., November 1982. Stress-strain characteristics of a low plasticity clay. Ph.D. thesis, Imperial College of Science and Technology, Univeristy of London.

Gens, A., Potts, D., 1988. Critical state models in computational geomechanics. Eng. Comput. 178, 178–197.

Hashiguchi, K., 1988. Mathematically consistent formulation of elastoplastic constitutive equations. In: Swoboda (Ed.), Numerical Methods in Geomechanics.

Hashiguchi, K., 2008. Verification of compatibility of isotropic consolidation characteristics of soils to multiplicative decomposition of deformation gradient. Soils and Foundations 48 (4), 597–602.

Holfz, R., Kovacs, W., 1985. An introduction to geotechnical engineering. Prentice-Hall.

Horne, M., 1965a. The behaviour of an assembly of rotund, rigid, cohesionless particles i. Proc. R. Soc. London. Ser. A. 286, 62–78.

Horne, M., 1965b. The behaviour of an assembly of rotund, rigid, cohesionless particles ii. Proc. R. Soc. London. Ser. A. 286, 79–97.

Houlsby, G., 1985. The use of a variable shear modulus in elastic-plastic models for clays. Comput. and Geotech. 1, 3–13.

Karstunen, M., Koskinen, M., 2008. Plastic anisotropy of soft reconstituted clays. Can. Geotech. J. 45, 314–328.

Karstunen, M., Krenn, H., Wheeler, S., Koskinen, M., Zentar, R., 2005. Effect of anisotropy and destructuration on the behavior of murro test embankment. Int. J. Geomech. ASCE 5 (2), 87–97.

Lade, P., Duncan, J., 1973. Cubical triaxial tests on cohesionless soil. J. Soil Mech. Found. Div. ASCE 99, 793–812.

Matsuoka, H., Nakai, T., 1974. Stress-deformation and strength characteristics of soil under three different principal stresses. Proc. JSCE 232, 59–70.

Maugin, G., 1992. The Thermomechanics of Plasticity and Fracture. Cambridge University Press.

Mróz, Z., Norris, V.A .and Zienkewicz, O., 1979. Application of an anisotropic hardening model in the analysis of elasto-plastic deformation of soils. Géotechnique 29, 1–34.

Muhunthan, B., Chameau, J., Masad, E., 1996. Fabric effects on the yield behaviour of soils. Soils Found. 36, 85–97.

Nouguier-Lehon, C., Cambou, B., Vincens, E., 2003. Influence of particle shape and angularity on the behaviour of granular materials: a numerical analysis. Int. J. Numer. Anal. Meth. Geomech. 27, 1207–1226.

Peña, A., Garcá-Rojo, R., Alonso-Marroquin, F., Herrmann, H., 2009. Investigation of the critical state in soil mechanics using dem. In: Nakagawa, M., Luding, S. (Eds.), 6th International Conference on the Micromechanics of Granular Media. pp. 185–188.

Peña, A., Garcá-Rojo, R., Herrmann, H., 2007. Influence of particle shape on sheared dense granular media. Granular Matter 9, 279–291.

Pestana, J., Whittle, A., 1999. Formulation of a unified constitutive model for clays and sands. Int. J. Numer. Anal. Meth. Geomech. 23, 1215–1243.

Potts, D., Zdravković, L., 2001. Finite element analysis in geotechnical engineering: Application. Thomas Telford Publishing, London.

Roscoe, K., Burland, J., 1968. On the generalised stress-strain behaviour of wet clay. In: Hayman, J., Leckie, F. (Eds.), Engineering Plasticity. Cambridge Univeristy Press, pp. 535–609.

Rothenburg, L., Kruyt, N., 2004. Critical state and evolution of coordination number in simulated granular materials. Int. J. Solids Struct. 41, 5763–5774.

Rouainia, M., Wood, D., 2000. A kinematic hardening constitutive model for natural clays with loss of structure. Géotechnique 50, 153–164.

Rouainia, M., Wood, D., 2001. Implicit numerical integration for a kinematic hardening soil plasticity model. Int. J. Numer. Anal. Meth. Geomech. 25, 1305–1325.

Shield, R., 1955. On coulomb's law of failure in soils. J. Mech. Phys. Solids 4, 10–16.

Sivasithamparam, N., Kamrat-Pietrasewska, D., Karstunen, M., 2010. An anisotropic bubble model for soft clays. In: 7th European Conference on Numerical Methods in Geoetchnical Engineering (NUMGE). pp. 21–26.

Wheeler, S., Näätänen, A., Karstunen, M., Lojander, M., 2003. An anisotropic elastoplastic model for soft clays. Can. Geotech. J. 40, 403–418.

Whittle, A., Kavvadas, M., 1994. Formulation of MIT-E3 constitutive model for overconsolidated clays. J. Geotech. Eng. 120 (1), 173–198.

Willam, K., Warnke, E., 1974. Constitutive model for the triaxial behaviour of concrete. In: Proceedings of the May 17-19 1974, International Association of Bridge and Structural Engineers Seminar on Concrete Structures Subjected to Triaxial Stresses, held at Bergamo Italy.

Yamakawa, Y., Hashiguchi, K., Ikeda, K., 2010. Implicit stress-update algorithm for isotropic cam-clay model based on the subloading surface concept at finite strains. Int. J. Plasticity 26 (5), 634–658.

Ziegler, H., 1983. An introduction to thermomechanics, 2nd Edition. North Holland Pub. Co, Amsterdam.

Zytynski, M., Randolph, M., Nova, R., Wroth, C., 1978. On modelling the unloading-reloading behaviour of soils. Int. J. Num. Ana. Meth. Geomech. 2, 87–94.
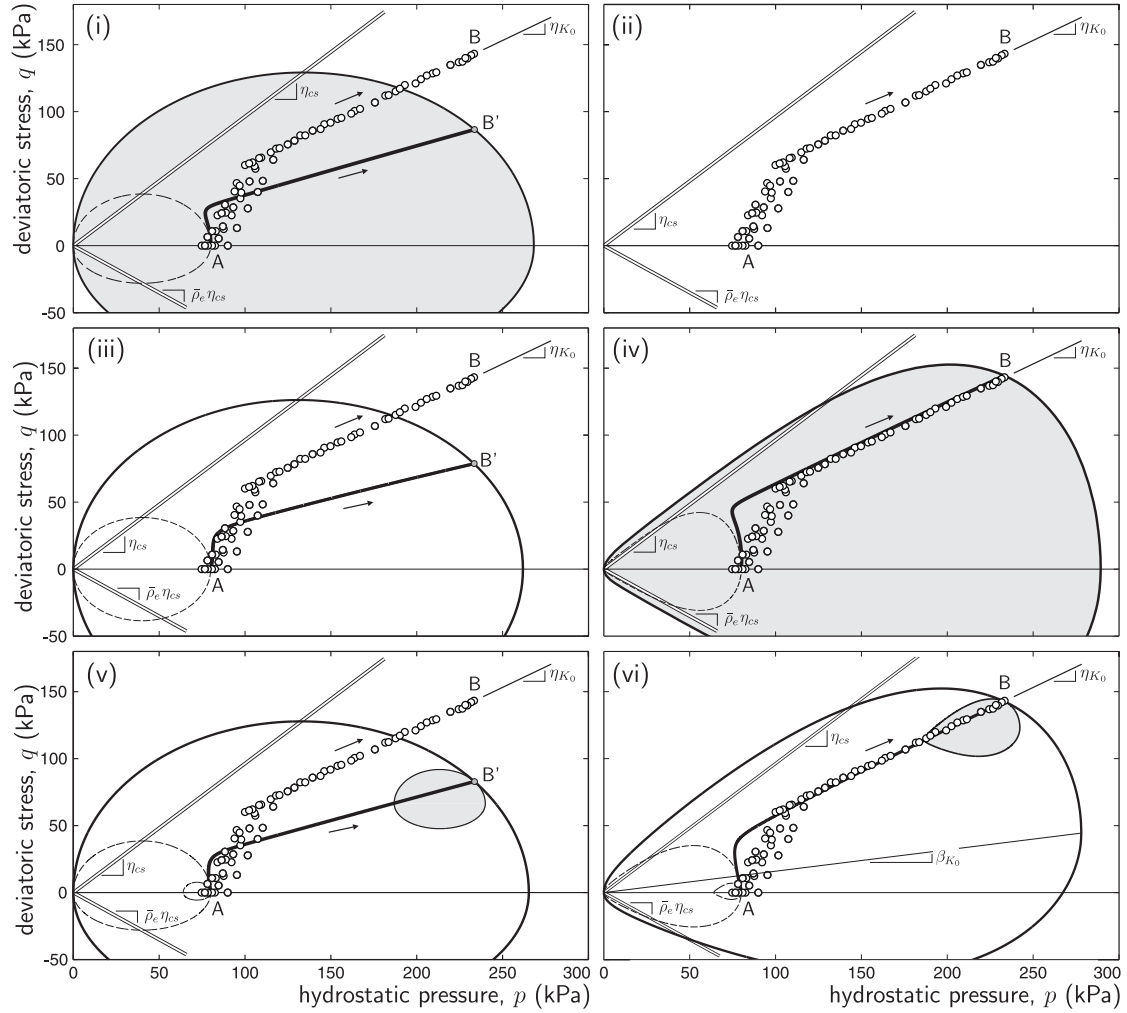
Figure 1: Two surface anisotropic model with $\eta_{cs} = 0.8$, $\alpha = 0.6$, $\gamma = 0.9$ and $\bar{\rho}_e = 0.7$: **(i)** in p-q stress space and **(ii)** deviatoric section through $p = p^\chi$. The LAD Critical State surface (CSS) and critical anisotropy surface (CAS) are identified in the deviatoric section.

Figure 2: One-dimensional (K_0) drained loading model predictions compared against experimental data (shown by discrete points) on LCT from Gens (1982): (i) MCC, (ii) SANIclay (Dafalias et al., 2006), (iii) anisotropic bounding surface (Borja et al., 2001), (iv) two-parameter isotropic (Coombs and Crouch, 2011), (v) two-surface "bubble" and (vi) the proposed two-surface anisotropic models. The shaded regions indicate the purely elastic zones.
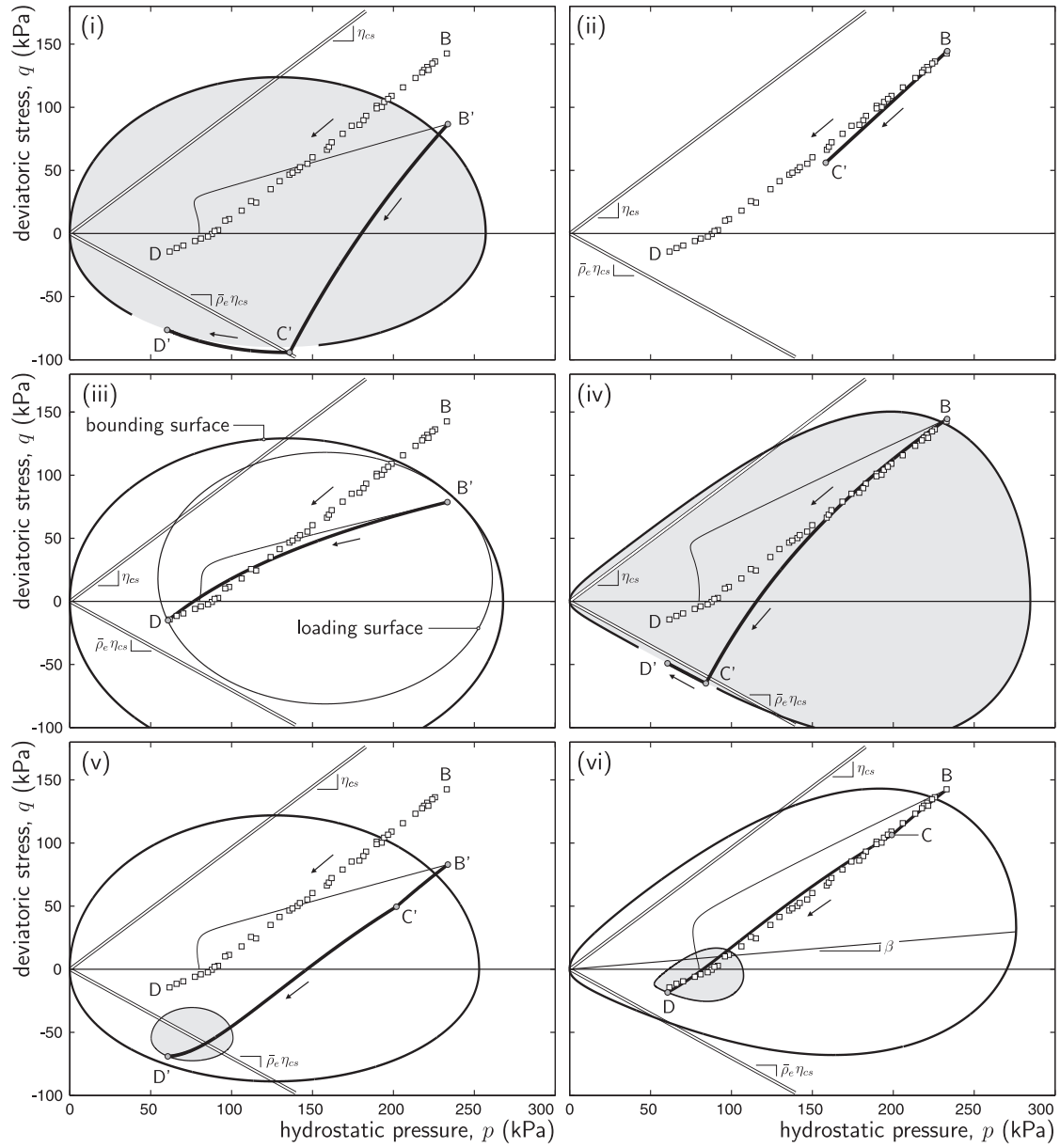
Figure 3: One-dimensional (K_0) drained unloading model predictions compared against experimental data (shown by discrete points) on LCT from Gens (1982): (i) MCC, (ii) SANIclay (Dafalias et al., 2006), (iii) anisotropic bounding surface (Borja et al., 2001), (iv) two-parameter isotropic (Coombs and Crouch, 2011), (v) two-surface "bubble" and (vi) the proposed two-surface anisotropic models. The shaded regions indicate the purely elastic zones.
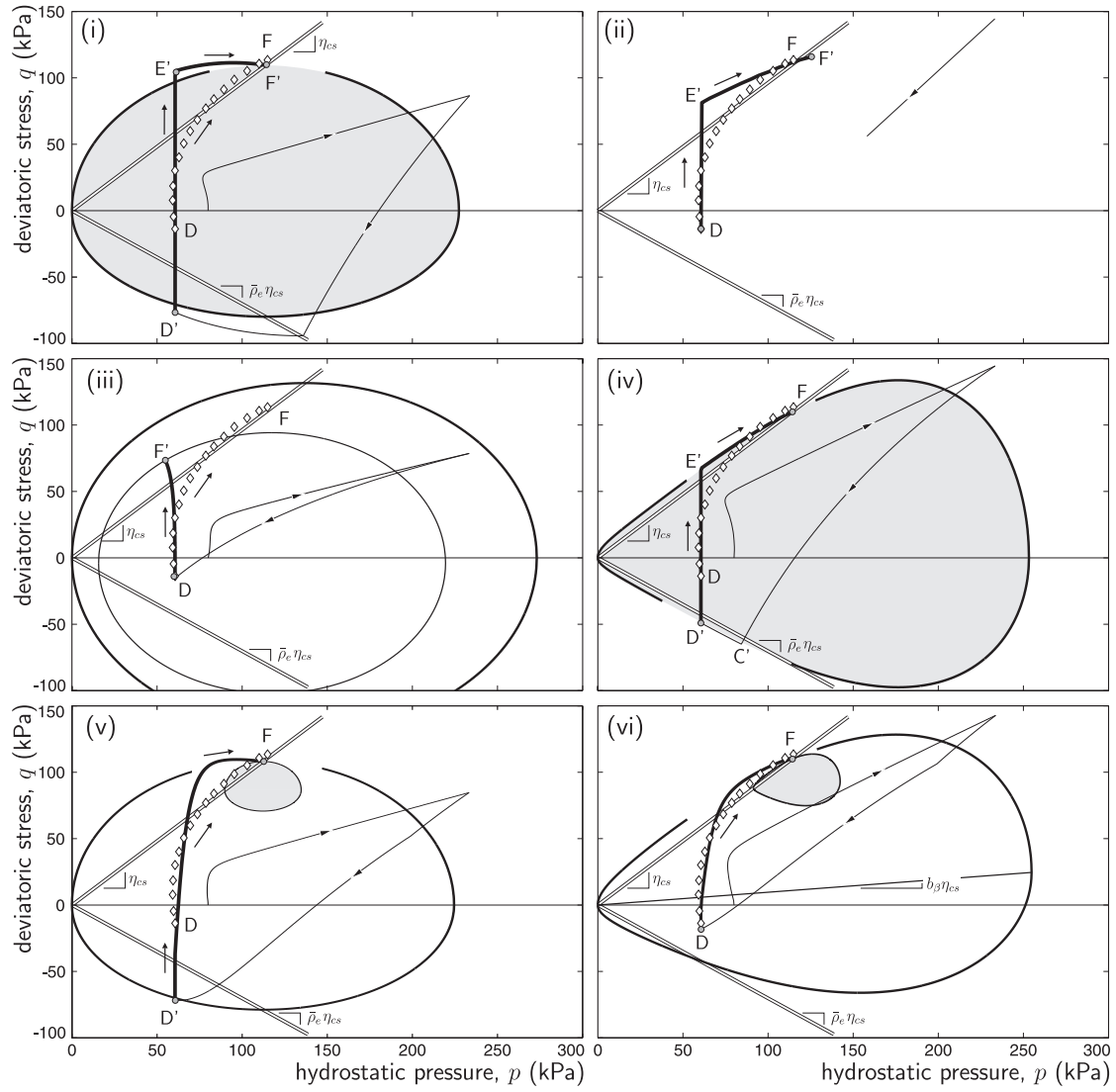
Figure 4: Undrained triaxial compression following one-dimensional loading and unloading model predictions compared against experimental data (shown by discrete points) on LCT from Gens (1982): (i) MCC, (ii) SAN-Iclay (Dafalias et al., 2006), (iii) anisotropic bounding surface (Borja et al., 2001), (iv) two-parameter isotropic (Coombs and Crouch, 2011), (v) two-surface "bubble" and (vi) the proposed two-surface anisotropic models. The shaded regions indicate the purely elastic zones.
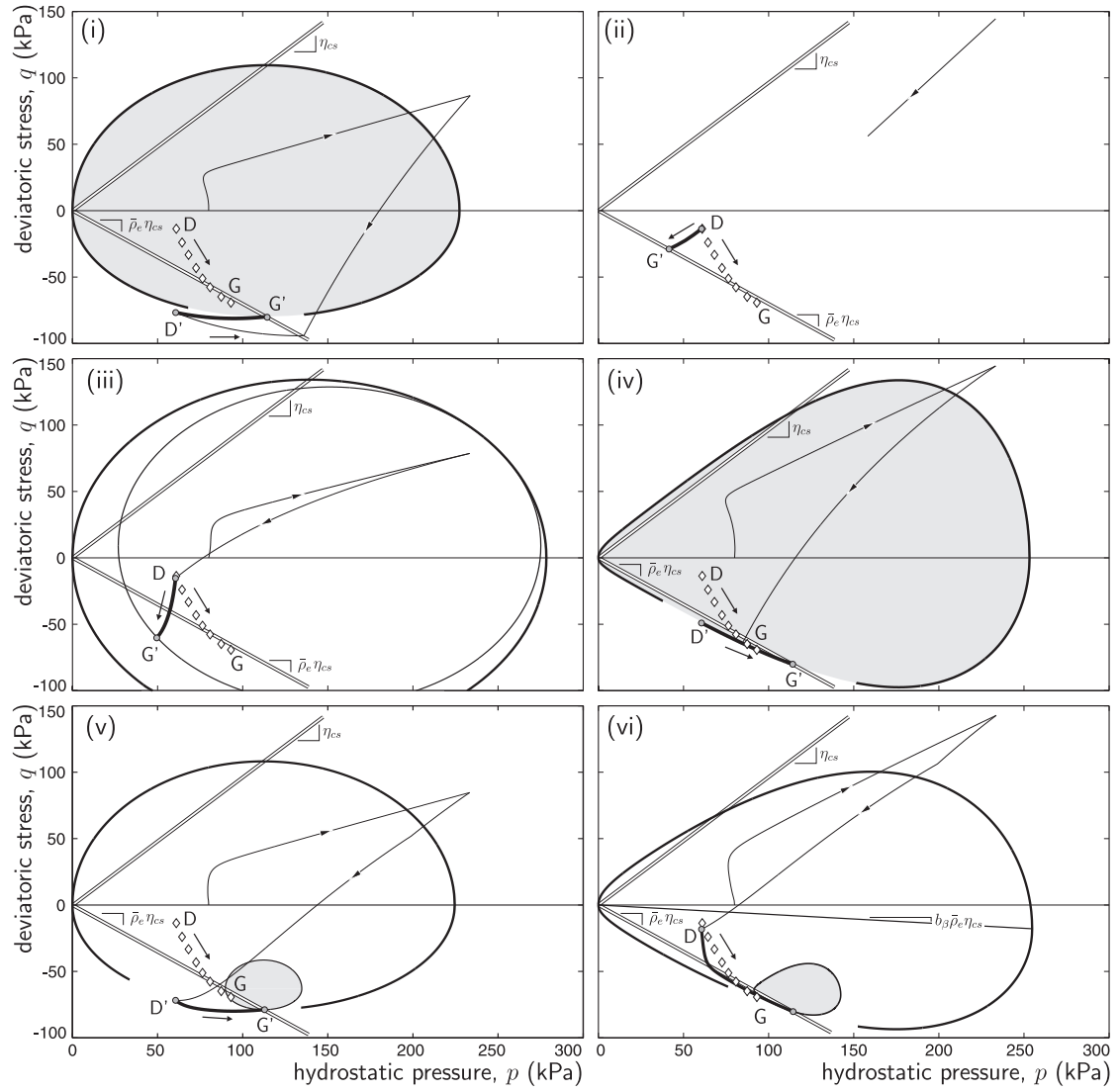
Figure 5: Undrained triaxial extension following one-dimensional loading and unloading model predictions compared against experimental data (shown by discrete points) on LCT from Gens (1982): (i) MCC, (ii) SANI-clay (Dafalias et al., 2006), (iii) anisotropic bounding surface (Borja et al., 2001), (iv) two-parameter isotropic (Coombs and Crouch, 2011), (v) two-surface "bubble" and (vi) the proposed two-surface anisotropic models. The shaded regions indicate the purely elastic zones.
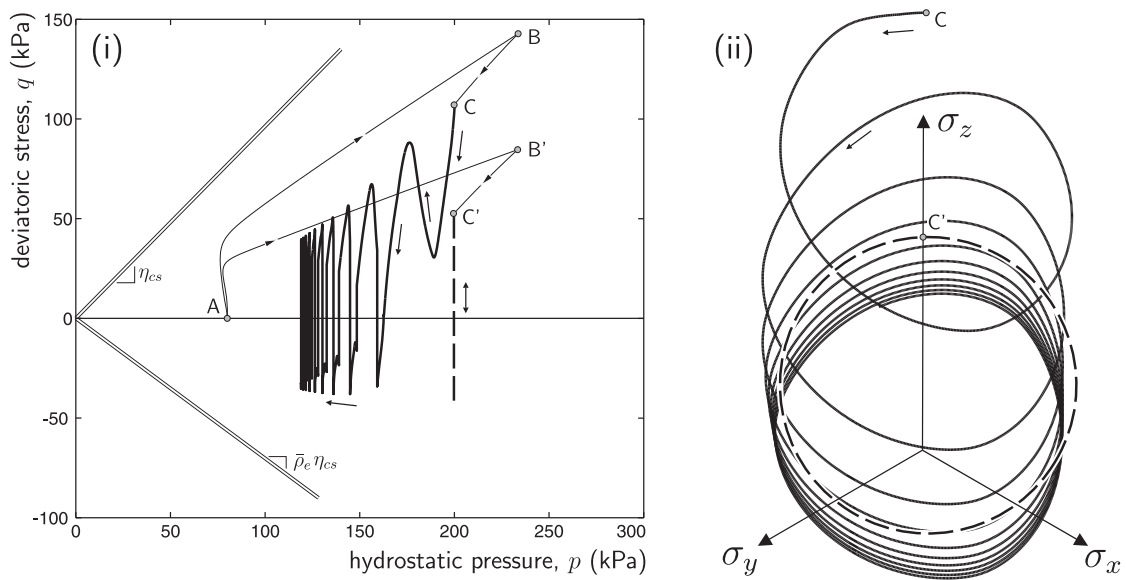
Figure 6: Rotating undrained strain path with a deviatoric radius of $1000\mu\varepsilon$: (i) q versus p space and (ii) three-dimensional normal stress space deviatoric view down the hydrostatic axis.

29

Appendix A. Lode angle dependency

The Lode angle, for the inner surface, is calculated from

$$\theta = \frac{1}{3}\arcsin\left(\frac{-3\sqrt{3}}{2}\frac{J_3}{J_2^{3/2}}\right) \quad \in \left[-\pi/6, \pi/6\right],\tag{A.1}$$

where $J_2 = \operatorname{tr}(s_{ij}^\beta s_{jk}^\beta)/2$ and $J_3 = \operatorname{tr}(s_{ij}^\beta s_{ij}^\beta s_{kl}^\beta)/3$.

Appendix B. Anisotropic Critical State

From the yield function and the direction of plastic flow, the position of the CS relative to the size of the yield surface is obtained as

$$(p_a)_{cs} = \frac{1 - b_\beta + b_\beta\gamma(2 - \gamma)}{b_\beta\gamma(2 - \gamma) + \gamma(1 - b_\beta)/2},\tag{B.1}$$

where $(p_a)_{cs} = p_s/p$. The value of M, required to maintain a given experimentally determined stress ratio at the CS, η_{cs}, is given by

$$M = \eta_{cs}\left(\frac{\left(1 - \gamma + \gamma(p_a)_{cs}/2\right)(1 - b_\beta)}{\left(1 - \alpha + \alpha\gamma(p_a)_{cs}/2\right)\sqrt{\gamma(2 - \gamma)\left((p_a)_{cs} - 1\right)}}\right).\tag{B.2}$$

Appendix C. One-dimensional anisotropy

For this calibration procedure, it is assumed that the elastic strains are negligible under sufficiently large K_0 straining. In this case, the ratio of the deviatoric to volumetric plastic strains (on the outer surface under triaxial conditions) is

$$\frac{\dot{\varepsilon}_\gamma^{\mathrm{p}}}{\dot{\varepsilon}_v^{\mathrm{p}}} = \frac{A^2(\eta_{K_0} - \beta)}{B^2(1 - \gamma p_a/2) - A^2(\eta_{K_0} - \beta)\beta} = n_p,\tag{C.1}$$

where η_{K_0} is the experimentally determined stress ratio (q/p) under K_0 loading, $p_a = p_c/p$, $\beta = \sqrt{\beta_{ij}\beta_{ij}}$ and $n_p = \sqrt{2/3}$. Assuming triaxial stress conditions, β can be obtained as

$$\beta = \eta - \frac{B}{A}\sqrt{\gamma(2 - \gamma)(p_a - 1)}.\tag{C.2}$$

Rearranging (C.1) and substituting for β from (C.2), a quartic in $(p_a)_{K_0}$ is obtained (as given by Coombs (2011)). Once solved for $(p_a)_{K_0}$, the asymptotic level of anisotropy under constant

K_0 loading can be calculated using (C.2).

Appendix D. Infinitesimal elasto-plastic stiffness matrix

The plastic consistency parameter is given by

$$\dot{\gamma} = \frac{(f,_\sigma)_{ji} D^e_{ijkl} \dot{\varepsilon}_{kl}}{(f,_\sigma)_{ab} D^e_{abcd} (g,_\sigma)_{cd} + H} \tag{D.1}$$

and is obtained using the four classical assumptions of plasticity theory, namely: additive strain decomposition, rate relationship between total stress and strain, plastic flow rule and the Kuhn-Tucker-Karush consistency conditions. $(f,_\sigma)_{ab}$ is the derivative of the yield function with respect to stress and the scalar measure of the plastic tangent stiffness, H, is given by

$$H = -(f,_\beta)_{ij}(H_\beta)_{ij} - (f,_{\sigma^\chi})_{ij}(H_{\sigma^\chi})_{ij} - f,_{p_c} H_{p_c}. \tag{D.2}$$

The instantaneous directions of plastic hardening, $H_{(\cdot)}$, are obtained from the hardening laws of p_c (6), β_{ij} (7) and σ^χ_{ij} (11) divided by the plastic multiplier rate, $\dot{\gamma}$. Combining these directions of instantaneous hardening with the direction of plastic flow (5), the derivative of the yield function with respect to stress and the elastic tangent stiffness matrix, we obtain the equations necessary to form the infinitesimal elasto-plastic tangent, relating infinitesimal changes in stress and strain, for the two-surface anisotropic model

$$D^{ep}_{ijkl} = D^e_{ijmn} \left[\delta_{mn}\delta_{kl} - \frac{(g,_\sigma)_{mn}(f,_\sigma)_{ab} D^e_{abkl}}{(f,_\sigma)_{ab} D^e_{abcd} (g,_\sigma)_{cd} + H} \right]. \tag{D.3}$$